Heliyon 9 (2023) e20746

Contents lists available at ScienceDirect

Heliyon

journal homepage: www.cell.com/heliyon

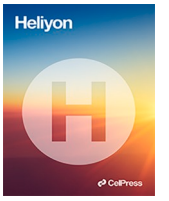

A Convergent fabrication of silk fibroin nanoparticles on quercetin loaded metal-organic frameworks for promising nanocarrier of myocardial infraction

Junjun Hao [a], Ankang Lv [b], Xingsheng Li [b], Yongyong Li [b,*]

[a] Department of Cardiovascular Surgery, First Affiliated Hospital of Xi'an Jiao Tong University, Xi'an-710061, China
[b] Department of Gerontology, the Second Affiliated Hospital of Chongqing Medical University, Chongqing-400010, China

ARTICLE INFO

Keywords:
Drug delivery
Myocardial infraction
pH-responsive
Zeolitic imidazolate framework-8 (ZIF-8)
Silk fibroin

ABSTRACT

The biomacromolecule silk fibroin (SF) may be constructed to promote biomimetic nucleation and nanostructures of inorganic nanomaterials, offering it a promising candidate for use in various biomimetic applications. We combined SF-NPs and ZIF-8-NPs to fabricate new drug vehicles that effectively release the drug. SF nanoparticles (SF-NPs) were assembled into quercetin (QCT), a myocardial drug added to fabricate QSF-NPs. By acting as a template for the ZIF-8 nucleation onto the surface, the QSF-NPs fabricated core-shell-structured nanocomposites (named QSF@Z-NCs) with ZIF-8 as the core-shell and the QSF-NPs. The biocompatibility analysis using the MTT assay revealed that the developed QCT, SF-NPs, and QSF@Z-NCs are not harmful to cardiac myoblast (H9C2) cells. The in vivo model demonstrated that H9C2 cells encouraged cardiomyocyte fibre regeneration in myocardial infarction rats. We fabricated a brand-new technique using H9C2 cells and QSF@Z-NCs that might encourage the healing processes in myocardial ischemia cells. This study's results demonstrate that it successfully treats myocardial injury.

1. Introduction

Stroke, atherosclerosis, and myocardial infarction (heart attack) are only a few examples of acute and chronic diseases that cause coronary artery constriction and blockage [1]. Yet, despite advances in treatment, cardiovascular disease is still the top cause of mortality worldwide [2]. Although cardiovascular disease has many potential causes, a common triggering factor is myocardial infarction (MI) due to acute or chronic ischemia [3]. Injury to tissues occurs quickly after a MI, and the pathologic remodeling of these tissues causes the cardiovascular disease to proceed rapidly [4]. Despite a consistent 20-year drop in the mortality rate, 2016 data still show that MI is directly responsible for 9.5 million fatalities annually. Additionally, individuals who do well after their initial MI are at a 20 % greater risk of requiring hospitalization again owing to a refractory MI or associated cardiac event [5]. Since Ischemic heart disease (IHD) affects roughly 153.5 million people worldwide, there is a pressing need to find effective treatments for a condition that places a heavy burden on healthcare resources, diminishes the quality of life for those who suffer from it, and claims too many lives [6].

MI causes extreme injury, and the heart's dysregulated cellular processes lead to more injury and unfavourable tissue remodeling

* Corresponding author. Department of Gerontology, the Second Affiliated Hospital of Chongqing Medical University, No.76 Linjiang Road, Yuzhong District, Chongqing, 400010, China.
E-mail address: yy_licqmu@163.com (Y. Li).

https://doi.org/10.1016/j.heliyon.2023.e20746
Received 4 July 2023; Received in revised form 29 September 2023; Accepted 5 October 2023
Available online 6 October 2023

[7]. Necrosis of cardiomyocytes (CMs) occurs in MI when coronary blood flow is cut off or decreased, generating a local hypoxic environment (ischemic injury) [8–10]. Infarct size is directly controlled by the time between when tissue is injured by ischemia and when blood flow is restored (reperfusion). Greater infarct size is associated with a decline in cardiac function and an exponential rise in the risk of developing heart failure [11]. However, reperfusion can unexpectedly worsen cardiac damage, a phenomenon known as Reperfusion injury (RI). Ruptured infarcts (RI) can contribute approximately 50 % of the total infarct size. Inflammation, Ca^{2+} excess, mitochondrial dysfunction, oxidative stress, and restoration of neutral pH are all potential causes of reperfusion damage [12]. Although promising approaches or new drugs for treating or preventing RI have been found via investigations in small animals, their efficacy has not been clearly shown in human clinical trials [13]. Many cellular processes break down, and tissue structure is severely damaged; the body cannot appropriately heal these problems after a MI. Therefore, there is inadequate management of, or prevention of, infarct size, a predictor of post-MI prognosis [14].

Due to its long history and tremendous applied energy, silk fibroin (SF) is a natural biopolymer energetically exploited in producing a wide range of medicinal materials, particularly in skin health maintenance and injury treatment [15]. When dealing with skin injuries with complicated scenarios (such as irregular-shaped wounds), it is necessary to use extra supplementary fixation, as standard SF wound dressings or wearables manufactured by procedures like spinning are pre-established and cannot adjust to deformation [16]. As a result, despite their adaptability, air permeability, and affinity to the skin, they provide nothing in the way of ease and versatility in application [17]. Considering this, the malleability of SF may be achieved by the methacrylate of SF branch chains, a modification technique previously developed for natural polymers like gelatin [18]. Alternatively, an earlier study shows that it may be equipped with dependable wet bonding properties by employing a biomimetic chemical modification strategy inspired by mussels [19]. Because of this, the SF can remain in place once they've been applied to the skin. New challenges arise in wound care despite the upgraded SF-state's advanced, quick flexibility and biological adhesion [20]. This is because an increase in moisture weakens the structural strength and raises the probability of bacterial growth [21].

The flavonoid quercetin (QCT) is abundant in various plant foods, including fruits, vegetables, leaves, and even certain Chinese herbs. Onions, apples, red wine, and tea are all foods that humans consume regularly that have significant concentrations of tannic acid [22]. It has anti-ageing, anti-aggregatory, anti-inflammatory, anti-cancer, and other biological properties [23]. Even at very high levels (4000 mg/day), QCT is non-toxic and safe for consumption. Indeed, in several nations, QCT has been purchased through local pharmacies for medical use [24]. In 2010, the 500 mg dose of QCT supplements was added to the Food and Drug Administration's (FDA) list of Generally Recognised as Safe (GRAS) supplements [25]. In addition, current evidence suggests that QCT offers significant therapeutic potential for reducing myocardial damage during ischemia and reperfusion (I/R) [26].

The mechanical strength of light-cured modified SF is essential for their practical application in skin care and as a guarantee for their biological-bonding capacity [27]. This method is excellent for modifying functional group protection. It is distinct from the traditional reinforcement from chemical crosslinking (such as ethanol or glutaraldehyde) because it is bio-friendly, safe, and ecologically acceptable [28]. Nano metal-organic frameworks (MOFs) serve a variety of roles as transporters, active additives, or sensors. They are thus projected to become beneficial in the structural augmentation of SF due to their high profile in the biomedical area [29]. Since metals and ligands self-assemble in predictable ways, MOF particles of the same kind can exhibit strikingly similar shapes and surface charges [30]. This quality of MOFs allows them to interact with natural polymers with different charges and branching groups, resulting in (like chitosan) more regular patterns and improved mechanical characteristics [31]. The microstructure of SF as a natural polymer may benefit from the potential-stabilizing action of MOFs since it has been shown that the more regularly ordered secondary protein structures are, the higher their mechanical strength. Therefore, modifying the structure of SF using nano MOFs is an exciting avenue for finding a middle ground between the two extremes of plasticity and dependability [32–34].

Our research first developed QSF-NPs by encapsulating QCT inside of SF-NPs. Zinc acetate and 2-methylimidazole, two precursors for ZIF-8, were then allowed to react with the QSF-NPs (HmIm). The QSF-NPs were modified by crystallizing ZIF-8-NPs on their surface to fabricated QSF@Z-NCs, which can govern the three-dimensional arrangement of zinc ions, like the SF-facilitated calcium ions regulation in the hydroxyapatite via biomimetic nucleation. We hypothesized that the ZIF-8-NPs shell would prevent the QCT release in a pH system. Both confirmed our results *in vitro* biocompatibility and an in vivo myocardial infraction investigation.

2. Materials and methods

2.1. Fabrication of QCT-loaded SF-NPs (QSF-NPs)

Following our prior protocol [15], SF was extracted from the B. mori cocoons and transformed into SF-NPs via precipitation. Over 30 min, 15 mL of an SF solution (3 mg/mL) was combined with 1 mL of isopropanol. Freeze-drying at 80 °C turned the liquid into a powder known as SF-NPs. The SF-NPs were diluted to 1 mg/mL with DI water to fabricate QSF-NPs, and an equivalent amount of stock solution of QCT was added. The combination was placed in mechanical shakers for a day at 37 °C and with constant shaking. For 10 min, samples were centrifuged at 6000 rpm while washed in DI water. The pellets obtained were then freeze-dried to fabricate QSF-NPs. To evaluate the encapsulation efficiency (EE) and drug loading content (LC). Using a standard curvature, the mass of QCT was analyzed from the absorbance of QCT in the supernatant at 510 nm.

2.2. Fabrication of QSF-NPs and QSF@Z-NCs

The QSF-NPs powder (4 mg) was dissolved in 2 mL of DI water, and then 2 mL of HmIm (60 mM) aqueous solution was added to fabricated ZIF-8-coated QSF-NPs (QSF@Z-NCs). ZIF-8-NPs coating was formed on the QSF-NPs by mixing the resulting solution with 2

mL of $Zn(NO_3)_2.6H_2O$ aqueous solution (5 mM) and shaking the mixture at 250 rpm for 15 min. After being separated by centrifugation, the QSF@Z-NCs were suspended in deionized water and freeze-dried to a powder. The formation of SF@Z-NCs followed the same protocol.

2.2.1. Fabrication of QSF@Z-NCs

To fabricate SF-loaded ZIF-8-NPs, a 100 μg/mL stock solution of QCT was combined with an equivalent amount of HmIm aqueous solution to make a 2 mL solution (60 mM). To fabricate DZ-NPs, we added 2 mL of a $Zn(NO_3)_26H_2O$ aqueous solution (5 mM) to the mixture and then shook it at 250 rpm for 15 min. The QSF@Z-NCs were filtered by centrifugation, then suspended in distilled water, and ultimately freeze-dried to fine powder sample.

2.3. Characterization of NPs

Fourier transform infrared spectroscopy (FTIR) was obtained with a Nicolet 67 spectrometer (Thermo Nicolet). The crystallography of NPs was analyzed using a mini-X-ray diffractometer with Cu Kα radiation (λ = 1.5418 Å, Japan). The morphology and structure of the as-fabricated NPs were examined using field emission transmission electron microscopes (TEM, Tecnai G2 20, Thermo) and field-emission scanning electron microscopy (SEM, ZEISS Sigma 300). Dynamic light scattering (DLS, Zetasizer Nano S, UK) was employed to establish the distribution of the hydrodynamic size of NPs. Fluorescence microscopy OLYMPUS X71 was used for fluorescence imaging.

2.4. Stability of QSF-NPs and QSF@Z-NCs aqueous suspensions

With some changes, the previously published approach was used to test NPs' colloidal stability [35]. Briefly, QSF-NPs and QSF@Z-NCs were kept in PBS solution (pH 7.4) for 35 days while gently shaking at 37 °C. After some time, the fabricated nanocomposite diameter and zeta potential were determined.

2.5. pH release of QCT from QSF-NPs and QSF@Z-NCs

To investigate QSF-NPs and QSF@Z-NCs released their QCT in pH 5.0 and 7.4, 10 mg nanocomposites were diluted into 8 mL. We measured the release efficacy by taking a 1 mL sample from the appropriate media and then adding a 1 mL sample of the new medium at 0, 1, 2, 3, 4, 5, 6, 7, and 8 days. A continuous release method was developed to mimic this transition since the NPs' natural habitat is in the acidic endosomes. Quickly, 8 days were spent storing PBS (8 mL, pH 7.4) containing either 10 mg of QSF-NPs or QSF@Z-NCs. The pH was then lowered to 6.0 using 0.6 M HCl, and the solution was stored for three days. Finally, the pH was brought down to 5.0, and the solution was stored for 6 days. Samples were taken daily, and the quantity of released QCT was determined. The samples were shaken at 150 rpm while the measurements were taken at 37 °C. QCT's mass was determined by fitting its absorbance at 510 nm.

2.6. In vitro biocompatibility of NPs

The cardiac myoblast (H9C2) cells were purchased from the Chinese Academy of Science (Shanghai, China). H9C2 cells were cultured in DMEM medium supplemented with 10 % (v/v) fetal bovine serum and penicillin-streptomycin (1 %) at 37 °C with 5 % CO_2.

In 96-well plates, 1×10^5 cardiac myoblast (H9C2) cells were grown using cell culture media after 1 day, 7 days, and 15 days, treated with QCT, SF-NPs, and QSF@Z-NCs. After different days, discarded the modified medium and cleaned the plates twice with PBS. To determine cytotoxicity, 200 μL of culture media and 20 μL of MTT (3-[4,5-dimethylthiazol-2-yl]-2,5 diphenyl tetrazolium bromide) were added to each well [36–40]. After 2 h, we measured the MTT at 450 nm for its absorbance [41]. The biocompatibility of the H9C2 cells was investigated in fluorescence microscopy using acridine orange (AO).

2.7. In vivo development of myocardial infraction

Forty-five SD rats weighing 200–250 g at eight weeks of age were used in this study and randomly assigned to one of four treatment groups (n = 5/group). All animal procedures were approved by the Animal Ethical Committee at the Second Affiliated Hospital of Chongqing Medical University and were conducted per the institution's "Guidelines for the Care and Use of Laboratory Animals." Isoflurane was used to induce anaesthesia in rats, and they were ventilated at 80 breaths per minute with a catheter. The anaesthetic effect of isoflurane was kept going at a 3 % concentration. The left coronary artery was ligated 2 mm from its origin using a polypropylene suture. The rats given acute myocardial injections were treated with various formulations 15 min after the arteries had been ligated. QCT, SF-NPs, and QSF@Z-NCs (200 μL) were injected with a 28-gauge needle along the peri-infarct zone in the specified area. Antibacterial penicillin was injected twice a day intramuscularly for three days after the injection, and the muscle and skin were sewn back together using double 10 proline sutures [42]. The mice were intravenously administered 1 mL of saline or 2 mg in saline solution of QCT, SF-NPs, and QSF@Z-NCs. The drugs were injected every three days for a total of three times via the tail vein. The mice intravenously injected with saline were included as controls. The body weights of the mice were monitored on day 30. For toxicity analysis, healthy ICR mice were intravenously injected with 1 mL of saline or 2 mg in saline solution of QCT, SF-NPs, and QSF@Z-NCs (200 μL). Blood samples (n = 5/group) were collected on day 9. Hepatorenal parameters, including white blood count (WBC), red blood cells (RBC), haemoglobin (HGB), platelets (PLT), mean corpuscular volume (MCV), mean corpuscular haemoglobin (MCH),

hematocrit (HCT), mean corpuscular haemoglobin concentration (MCHC) were analyzed.

2.8. Histological studies

Four weeks after being administered with a combination of 1.5 % isoflurane and oxygen (0.8 l/min), rats in both the treatment and control groups were euthanized. The 3–5 mm thick heart tissues were carefully removed, fixed in 4 % paraformaldehyde at 4 °C, and stained with H&E staining [43].

2.9. Statistical analysis

Data are presented as mean ± standard deviation (SD). The statistical significance between groups was assessed using one-way ANOVA with GraphPad Prism 9.0 software. Statistical significance was established at $P < 0.05$, where * $P < 0.05$; ** $P < 0.01$; *** $P < 0.001$, and **** $P < 0.0001$.

3. Results and discussion

3.1. Characterization of NPs

Worldwide, myocardial infarction is a leading cause of death and disease. Regenerative treatments have not achieved considerable progress due to the adult mammalian myocardium's weak intrinsic regeneration and challenges with efficient drug delivery [44]. Enhanced delivery, retention, and sustained therapeutic efficacy are just a few of the possible benefits that nanocarriers, such as exosomes, nanoparticles, and liposomes, might provide for the treatment of myocardial infarction [45–47]. Various issues have hampered the broad application of these technologies in clinical settings. Hence, we developed SF nanoparticles (SF-NPs) assembled into quercetin (QCT), a myocardial drug that was added to fabricate QSF@Z-NCs for myocardial infarction.

The particle size distributions of SEM and TEM for both SF-NPs (~200 nm) and QSF@Z-NCs (~220 nm) were quite well-dispersed (Fig. 1A and B). DLS analysis verified the SF-NPs and QSF@Z-NCs reported sizes (Fig. 2B). However, XRD analysis confirmed the presence of ZIF-8-NPs diffraction peaks in the SF@Z-NPs (Fig. 2A). These findings established that ZIF-8 was accumulated on the surface of SF-NPs to fabricate QSF@Z-NCs, which possessed a core-shell architecture. QCT has shown that the positive charge has been effectively encapsulated into the SF-NPs. The zeta potential surface charges were roughly −7 and +5 mV, respectively. Also, the synthesis of ZIF-8-NPs surface of QSF-NPs into QSF@Z-NCs resulted in an elevation, and the zeta potential of QSF@Z-NCs shows 18 mV. (Fig. 2C). The peaks at 680, 750, and 1140 cm^{-1} seen in the FTIR spectrum of the SF@Z-NPs are consistent with ZIF-8-NPs (Fig. 3). Thus, our findings demonstrated that SF@Z-NPs might be successfully prepared.

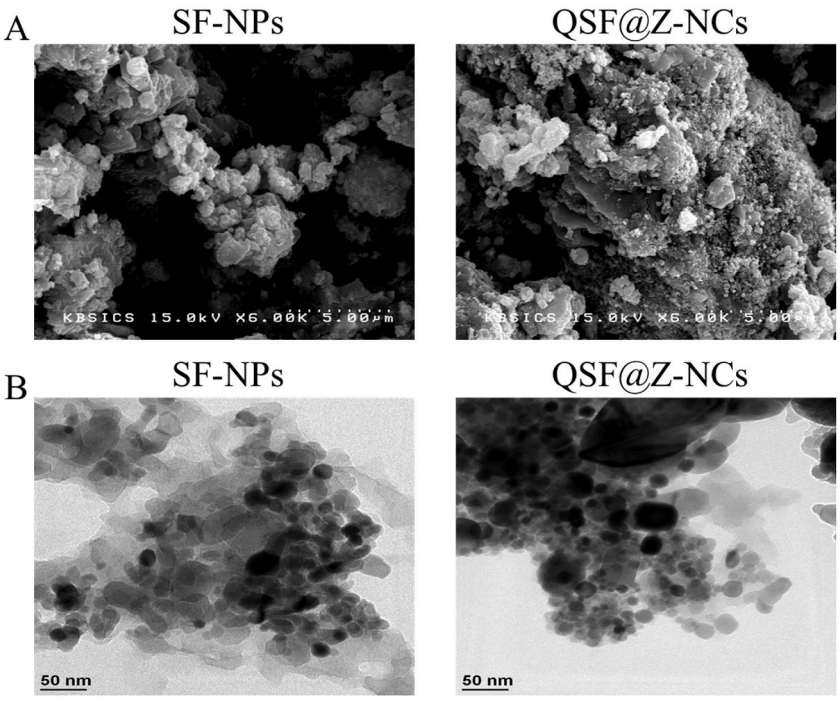

Fig. 1. Characterization of various nanoparticles. (A) SEM images of the SF-NPs and SF@Z-NPs. Scale bar: 5 μm. (B) The TEM image of SF-NPs and QSF@Z-NCs. Scale bar: 50 nm.

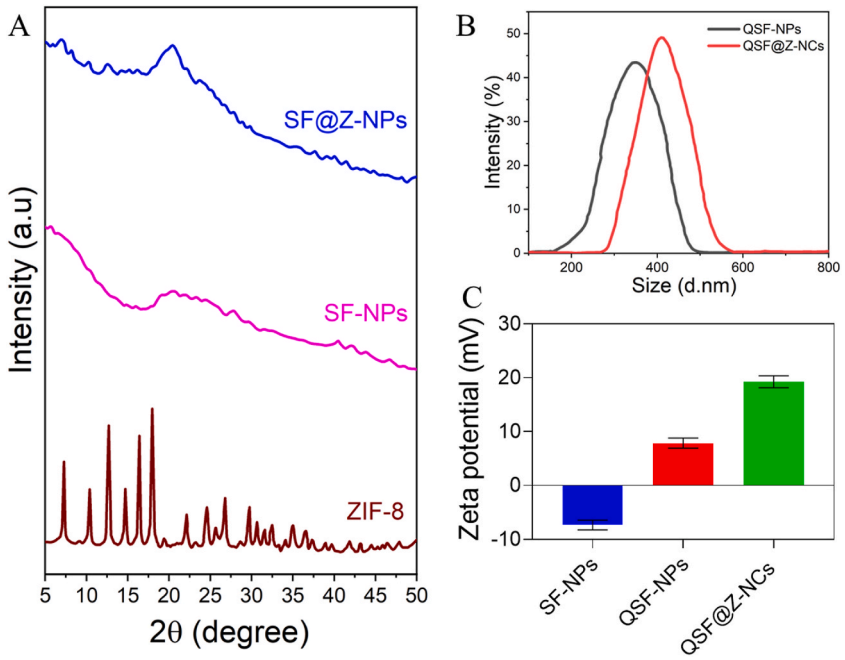

Fig. 2. (A) Powder XRD patterns of ZIF-8, SF-NPs, and SF@Z-NP. (B) Particle size distribution of QSF-NPs and QSF@Z-NCs. C) Zeta potential of SF-NPs, QSF-NPs, and QSF@Z-NCs. Data represented as mean ± SD of three independent experiments (n = 3).

The QSF-NPs and QSF@Z-NCs were stopped in PBS and gently shaken for 35 days at 37 °C to verify their colloidal stability. Colloidal particles did not aggregate throughout this time, and neither particle size nor zeta potential changed noticeably (Fig. 4A and B). According to the findings, NPs exhibited acceptable levels of colloidal stability.

The QSF@Z-NCs' permanent porosity was determined using N_2 adsorption. A reversible type II isotherm was observed in QSF@Z-NCs (Fig. 4C). Using the BET model, we determined the surface area of the various samples. The ZIF-8-coated SF@Z-NPs had a higher BET surface area than uncoated SF-NPs (from 103 to 170 $m^2\ g^{-1}$), indicating improved reaction area. The encapsulation of QCT in QSF@Z-NCs was confirmed by the fact that the BET surface region of QSF@Z-NCs was reduced with increasing QCT loading. Fig. 4D displays the porous size and porous volume dispersal of NPs determined utilizing the BJH method. The pore sizes of all samples were similar, with no statistically significant deviations. However, BET surface area data showed that SF@Z-NPs had the highest pore volume (0.36 $cm^3\ g^{-1}$) compared to QSF@Z-NCs, which had the smallest (0.19 $cm^3\ g^{-1}$). As previously discussed [48], incorporating ZIF-8-NPs into SF@Z-NPs may increase pore volume and surface area. The loaded QCT into both the QSF@Z-NCs surface and pore volume.

3.2. pH-release and drug loading of QCT from QSF@Z-NCs

Under the QCT concentration, the drug's LC increased while the EE decreased. QCT concentrations of about 70 μg/mL, LC, and EE peaking at around 6.0 and 87.1 %, respectively (Fig. 5). The high EE can be attributed to the numerous carboxy-terminal and amino groups of SFs, which allow the SF to absorb and deceive the QCT efficiently. In addition, SF's net negative charge adds to the QCT binding's positive charge. These characteristics make SF-NPs permeable to QCT. QSF-NPs (Fig. 5) and QSF@Z-NCs (Fig. 5) released QCT at a greater rate in the first few hours but at a more regulated pace in the latter hours when pH was set to 5.0. QSF-NPs and QSF@Z-NCs discharged over 90 % of their loaded QCT after 8 days. 60 % of the loaded QCT was released from the QSF-NPs after 8 days when the pH was adjusted to 7.4. However, after being coated with ZIF-8, QSF@Z-NCs exhibited a prolonged slow release throughout the method, with only 31 % of QCT released at pH 7.4 by day 8, demonstrating that ZIF-8-NPs on QSF@Z-NCs improved their neutral environment constancy. QSF@Z-NCs pH sensitivities were further validated by their continuous release. When the pH was lowered from 7.4 to 6.0 to 5.0, the study found that the QCT was barely released gradually. After 10–20 days, NPs released around 50 % of their stored QCT (Fig. 6A). These findings corroborated previous research showing that QSF@Z-NCs is a potential pH-responsive DDS [49]. The presence of Zn in the PBS supernatants (Fig. 6B) indicated that Zn^{2+} were liberated from ZIF-8-NPs. These results suggested that the drug release of QSF@Z-NCs in an acidic setting was undoubtedly initiated by the breakdown of ZIF-8, which acted as the QSF@Z-NCs. As opposed to that, QSF@Z-NCs safely held QCT without any release under physiological settings.

3.3. In vitro studies

Drug safety is a critical clinical parameter. Cardiac myoblast (H9C2) cells were used for cytotoxicity testing by using QCT, SF-NPs,

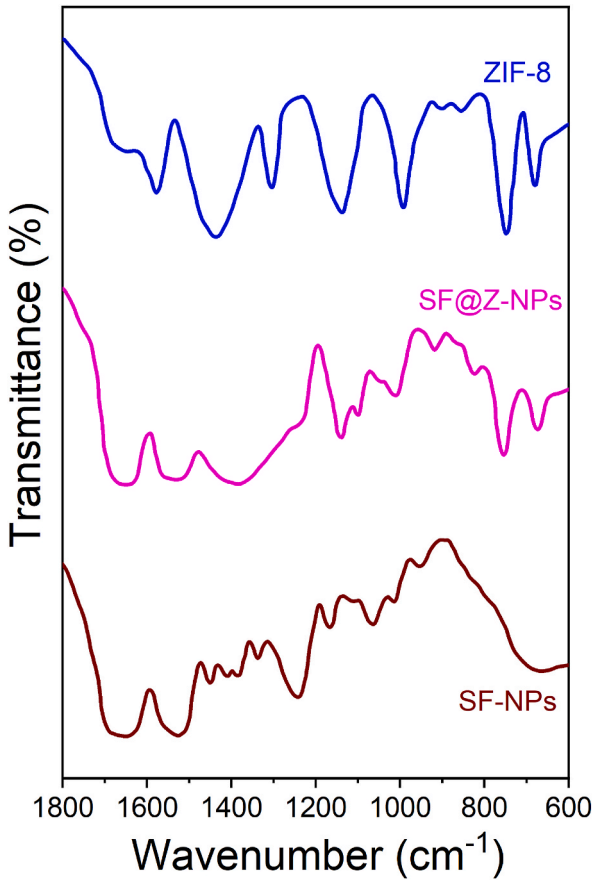

Fig. 3. FTIR spectral analysis of ZIF-8, SF@Z-NPs, and SF-NPs.

and QSF@Z-NCs compared with positive control to address that factor. No toxicity to normal cells was observed for day 1, day 5, and day 15, as illustrated in Fig. 7. Also, cells grown in standard media or circumstances containing QCT, SF-NPs, and QSF@Z-NCs showed no discernible differences. As with other cell lines tested for cytotoxicity, H9C2 cells were subjected to the MTT assay. On day one, the viability of cultivated H9C2 cells ranged from 53 % to 66 %, but on day 15, it increased from 71 % to 89 %. (Fig. 7). After 15 days, this activity level exceeded that of cell treatment alone (93 %) for QSF@Z-NCs. As shown in Fig. 7, the percentage of cell viability following treatment with QCT, SF-NPs, and QSF@Z-NCs, and cells was very close to the MTT assay results. QSF@Z-NCs were non-toxic to H9C2 cells, indicating their potential usefulness in medical settings. Platelet adhesiveness after treatment with QCT, SF-NPs, and QSF@Z-NCs was examined *in vitro* using the method depicted in Fig. 7. As time increased from day 1 to day 15, the results showed that the QSF@Z-NCs group had considerably higher cell proliferation than the QCT and SF-NPs.

The viability results from the fluorescence microscopic images confirmed that fabricated QSF@Z-NCs survival percentages of 93% on day 15 showed that QCT and SF-NPs did not damage the cell morphology and membrane during the cell culture with different days. Fig. 8A–C shows microscopic images of QCT, SF-NPs, and QSF@Z-NCs migrations on days 1 (Figs. 8A), 7 (Fig. 8B), and 15 (Fig. 8C). It demonstrates that cells treated with QSF@Z-NCs have been grown and migrated well, like the QCT, SF-NPs, which indicates accumulation of amino acids and carboxylic groups of the nanocomposites, which influence the cell growth on different days. The excellent cell proliferation ratio indicated the percentage of cell growth matched the improving fibroblast culture days and the nanocomposite surface advantages for strong cell proliferation. Combining the cell growth and proliferation ratio on the QSF@Z-NCs is high and promising uses for the clinical application compared to the QCT, and SF-NPs.

3.4. In vivo studies

Histochemical analysis employing H&E staining was performed on nuclear, collagenous, and cytoplasmic areas of ischemia and treated heart tissue sections (Fig. 9). Fig. 9A–D shows the morphologies of the blue collagen in the infarcted area, demonstrating a severely infarcted myocardial. Myofibers with central nuclei revealed that cardiac muscle fibres were healing in cell-treated MI heart tissue, but this recovery was modest. QSF@Z-NCs also promoted the regeneration of cardiac muscle fibres. In contrast, in areas treated with QCT, SF-NPs, and QSF@Z-NCs, cells showed much better fibres and less stained collagens than in untreated areas. The QSF@Z-NCs group provided strong evidence that the restored cardiac tissues following cell implantations were functional (Fig. 9A–D).

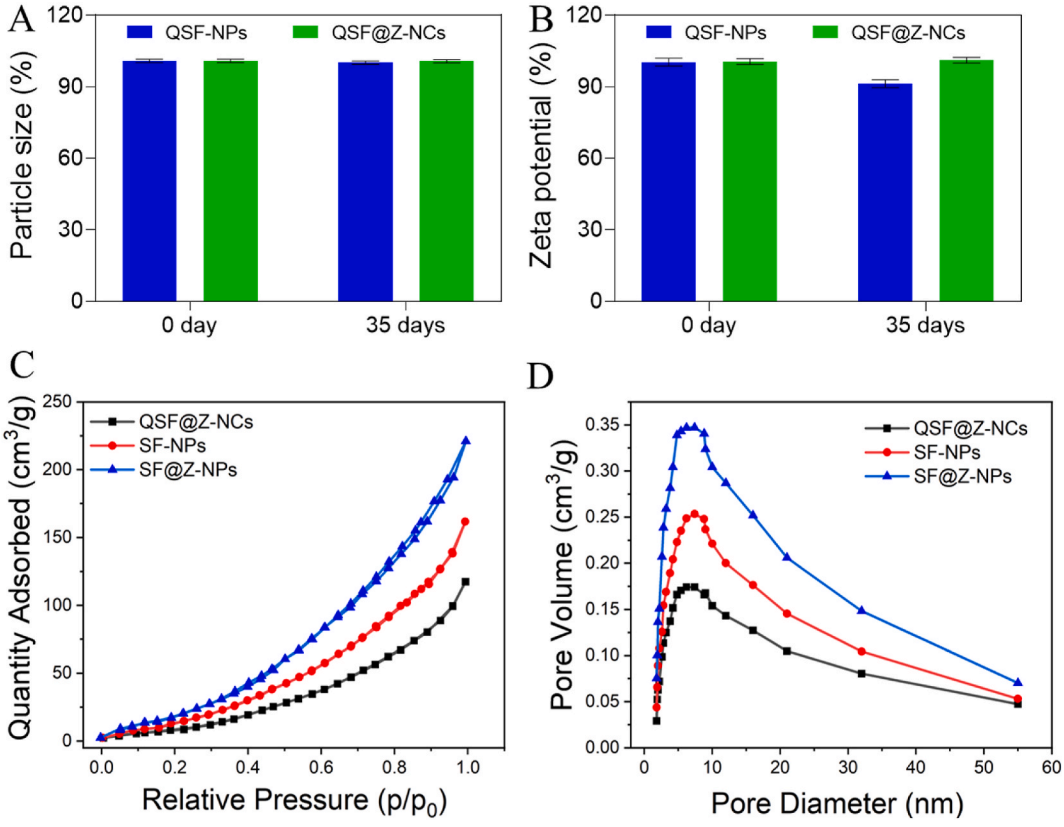

Fig. 4. Colloidal stability and porosity of QSF@Z-NCs for over 35 days. (A and B) Effect of storage time on QSF-NPs and QSF@Z-NCs. Data represented as mean ± SD of three independent experiments (n = 3). C) N_2 adsorption isotherm of SF-NPs, QSF-NPs, and QSF@Z-NCs. (D) Pore size distributions for SF-NPs, QSF-NPs, and QSF@Z-NCs were determined utilizing the BJH method.

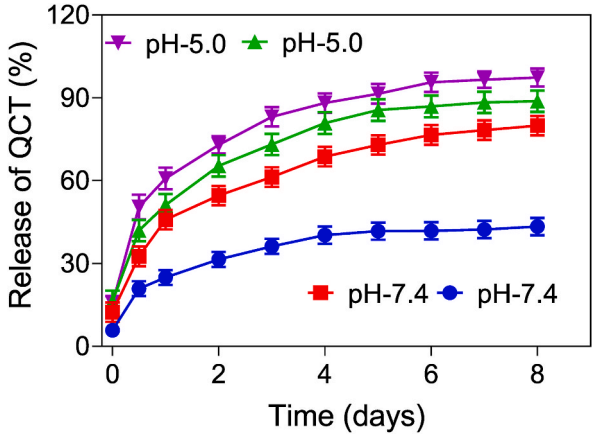

Fig. 5. Controlled QCT release from QSF@Z-NCs in response to acidic pH. QCT release in pH-5.0 and pH-7.4 media from QCT-NPs (purple and red) and DSF@Z-NPs (green and blue), indicating the controlled QCT release from QSF@Z-NCs selectively under acidic pH. Data represented as mean ± SD of three independent experiments (n = 3). (For interpretation of the references to colour in this figure legend, the reader is referred to the Web version of this article.)

However, the minimal fibrosis area was found in the cultured with QSF@Z-NCs cells treatment, suggesting the therapeutic influence of nanoparticles loaded QCT and SF-NPs with cells.

After 30 days of obtaining the intravenous injection of QCT, SF-NPs, and QSF@Z-NCs at a 2 mg/mouse dosage, white blood count (WBC), red blood cells (RBC), haemoglobin (HGB), platelets (PLT), mean corpuscular volume (MCV), mean corpuscular haemoglobin (MCH), hematocrit (HCT), mean corpuscular haemoglobin concentration (MCHC) tests were performed to assess in vivo

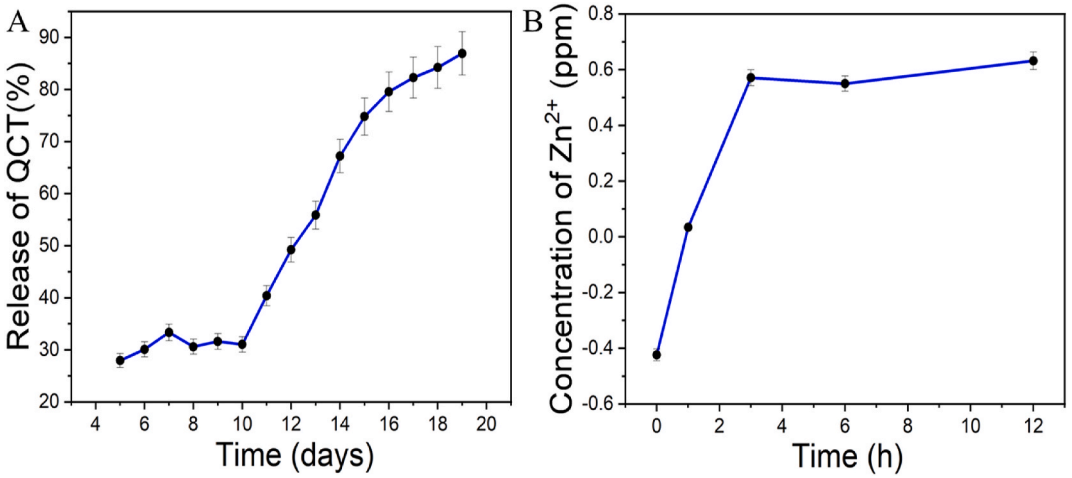

Fig. 6. A) QCT release profiles of QSF@Z-NCs. B) Concentrations of Zn^{2+} in the supernatants of the release medium at pH 5.0 for different time points of release. Data represented as mean ± SD of three independent experiments (n = 3).

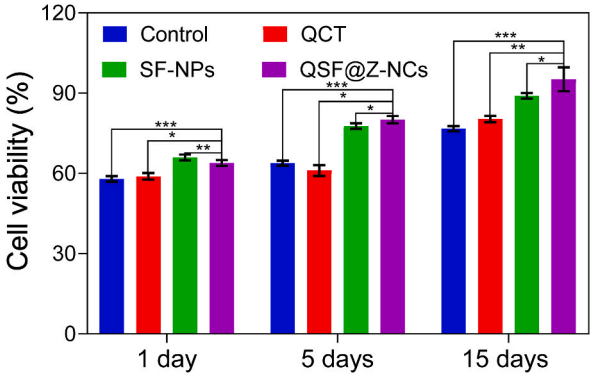

Fig. 7. Cell proliferation analysis of cell survival of H9C2 fibroblast cells treated with QCT, SF-NPs, and QSF@Z-NCs at 1, 7, and 15 days. Data represented as mean ± SD of three independent experiments (n = 3). The significance levels were set at probabilities of *p < 0.05, **p < 0.01, and ***p < 0.001.

hemocompatibility. As shown in Fig. 10A–H, the haematological findings of the group treated with control (saline) QCT, SF-NPs, and QSF@Z-NCs showed no significant changes from the saline-injected control group. While no apparent differences were detected in the WBC, RBC, PLT, MCV, MCH, HCT, and MCHC ratio between the QSF@Z-NCs and saline groups, confirming that QSF@Z-NCs had no toxicity in mice (Fig. 10A–H). This confirms QSF@Z-NCs' nature and tiny particle size, which had no detrimental effects on mice models and are incredibly beneficial for pharmacological and biomedical purposes.

4. Conclusions

Here, we describe an innovative approach to development and potential therapeutic fabrication using injectable QSF@Z-NCs, bolstered by a culture of H9C2 cells. SF nanoparticles (SF-NPs) were assembled into quercetin (QCT), a myocardial drug added to fabricate QSF-NPs. The biocompatibility analysis using the MTT assay revealed that the developed QCT, SF-NPs, and QSF@Z-NCs are not harmful to cardiac myoblast (H9C2) cells. The in vivo model demonstrated that H9C2 cells encouraged cardiomyocyte fibre regeneration in myocardial infarction rats. Improved cardiac development in treated cells may help to overcome electrophysiological barriers and deliver cytokines that benefit the heart. QSF@Z-NCs groups were fabricated and used in the cells in rat models of myocardial infarction, which may have improved cardiac tissue regeneration and functional recovery. The study found that QSF@Z-NCs and H9C2 provided adequate material for cardiac tissue engineering applications.

Funding statement

This work was supported by the Nan'an District of Chongqing Science and Health Joint Medical Research Project (Project No.: 2021-07).

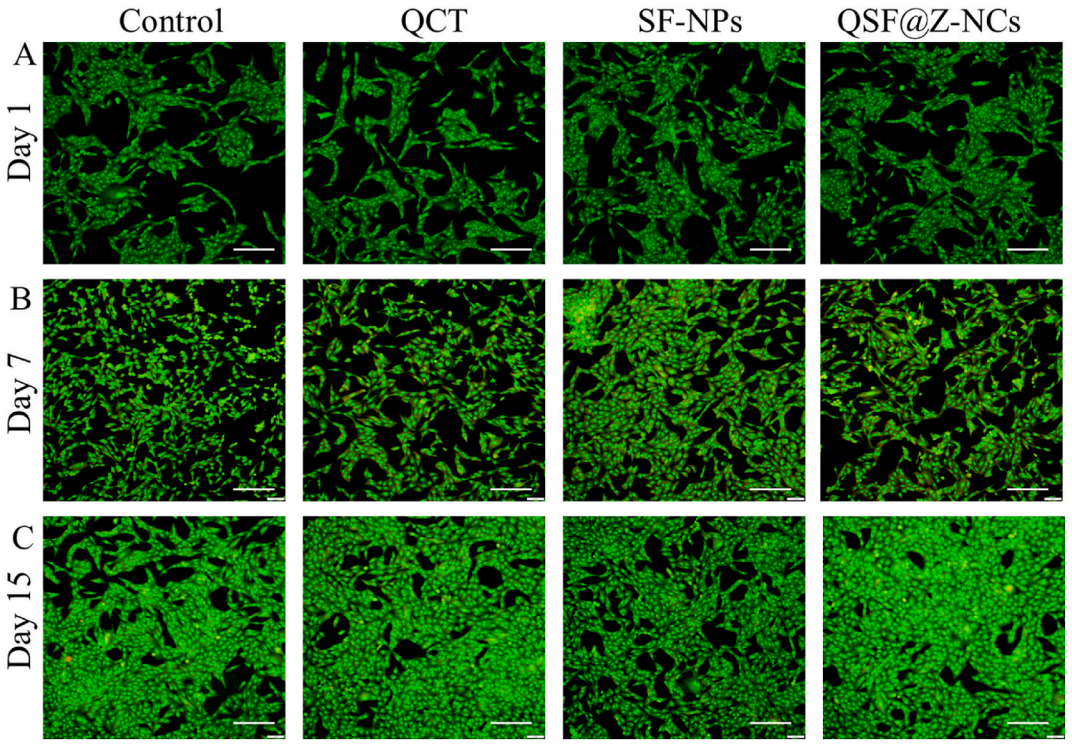

Fig. 8. Cell viability images of the samples. Fluorescence microscopic images of H9C2 fibroblast cells treated with QCT, SF-NPs, and QSF@Z-NCs at 1 (A), 7 (B), and 15 (C) days. Scale bar 20 μm.

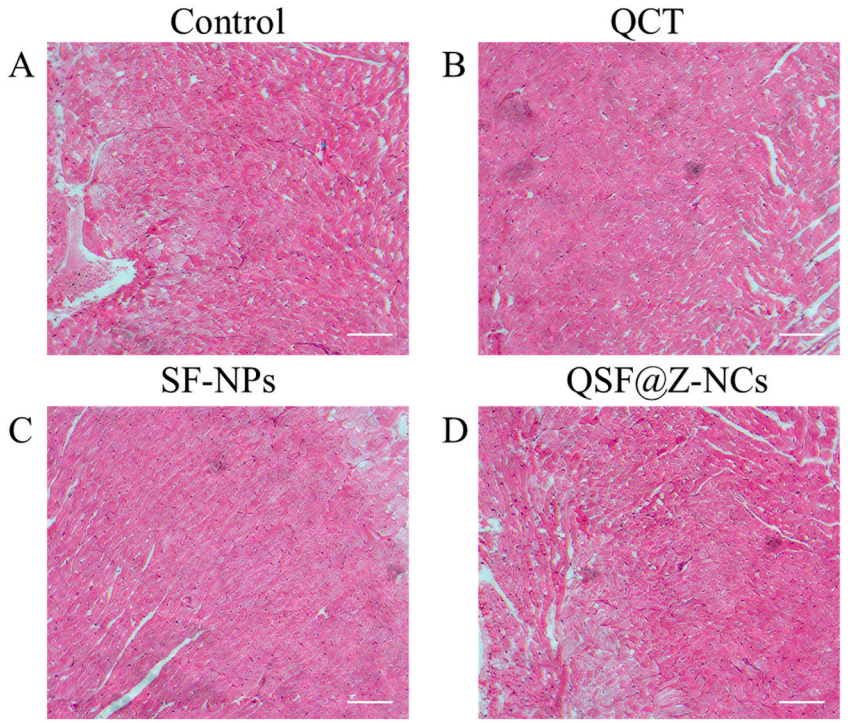

Fig. 9. Myocardial histological images of the samples. The cardiac configuration of infarcted hearts with control (A), QCT (B), SF-NPs (C), and QSF@Z-NCs (D) therapy in vivo. Histology (H&E) analysis of hearts for the control and different treatment groups. Scale bar 100 μm.

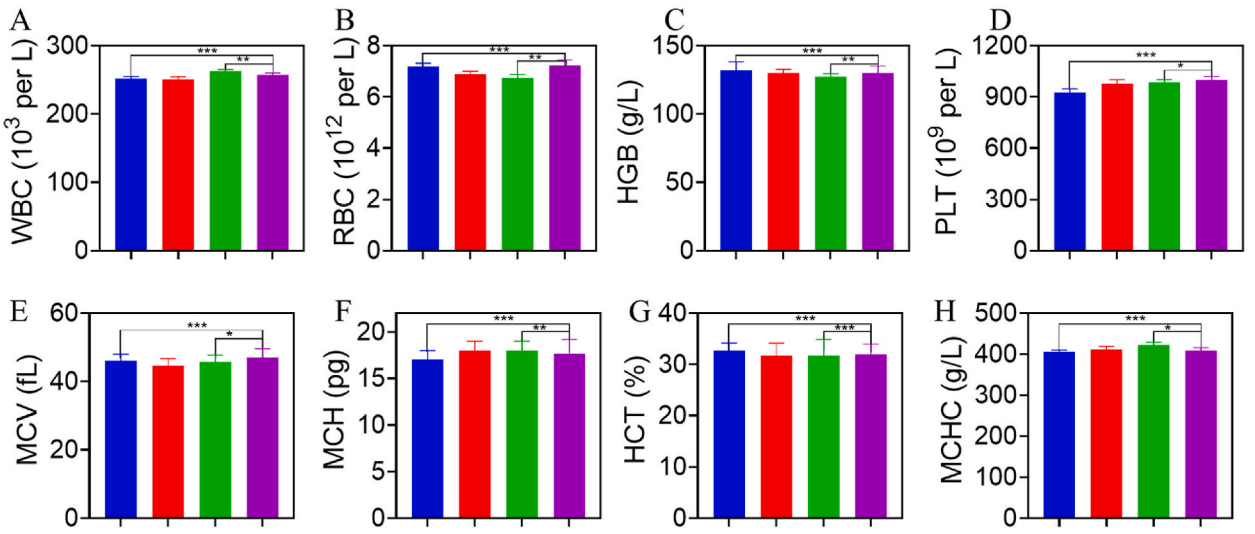

Fig. 10. Blood biochemical assay and haematology analysis. The mice 30 days after the intravenous injection of saline (control group), QCT, SF-NPs, and QSF@Z-NCs. A) White blood count (WBC), B) Red blood cells (RBC), C) Haemoglobin (HGB), D) Platelets (PLT), E) Mean corpuscular volume (MCV), F) Mean corpuscular haemoglobin (MCH), G) Hematocrit (HCT), H) Mean corpuscular haemoglobin concentration (MCHC). Data represented as mean ± SD of three independent experiments (n = 5). The significance levels were set at probabilities of *$p < 0.05$, **$p < 0.01$, and ***$p < 0.001$. (For interpretation of the references to colour in this figure legend, the reader is referred to the Web version of this article.)

Data availability statement

Data will be made available on request.

Ethics approval and consent to participate

This research was approved by The Second Affiliated Hospital of Chongqing Medical University Animal Ethical Committee, Approved No.(2021)667.

CRediT authorship contribution statement

Junjun Hao: Conceptualization, Formal analysis, Investigation, Writing – original draft. **Ankang Lu:** Conceptualization, Data curation, Formal analysis, Investigation, Writing – original draft. **Xingsheng Li:** Resources, Software, Visualization. **Yongyong Li:** Project administration, Writing – review & editing.

Declaration of competing interest

The authors declare that they have no known competing financial interests or personal relationships that could have appeared to influence the work reported in this paper.

References

[1] D. Jenča, V. Melenovský, J. Stehlik, V. Staněk, J. Kettner, J. Kautzner, V. Adámková, P. Wohlfahrt, Heart failure after myocardial infarction: incidence and predictors, ESC Heart Failure 8 (2021) 222–237.
[2] B. Vogel, B.E. Claessen, S. V Arnold, D. Chan, D.J. Cohen, E. Giannitsis, C.M. Gibson, S. Goto, H.A. Katus, M. Kerneis, ST-segment elevation myocardial infarction, Nat. Rev. Dis. Prim. 5 (2019) 39.
[3] M. Saleh, J.A. Ambrose, Understanding myocardial infarction, F1000Research 7 (2018).
[4] H.D. White, D.P. Chew, Acute myocardial infarction, Lancet 372 (2008) 570–584.
[5] G.W. Reed, J.E. Rossi, C.P. Cannon, Acute myocardial infarction, Lancet 389 (2017) 197–210.
[6] N.G. Frangogiannis, C.W. Smith, M.L. Entman, The inflammatory response in myocardial infarction, Cardiovasc. Res. 53 (2002) 31–47.
[7] L. Sarkisian, L. Saaby, T.S. Poulsen, O. Gerke, N. Jangaard, S. Hosbond, A.C.P. Diederichsen, K. Thygesen, H. Mickley, Clinical characteristics and outcomes of patients with myocardial infarction, myocardial injury, and nonelevated troponins, Am. J. Med. 129 (2016), 446-e5.
[8] R.L. McNamara, K.F. Kennedy, D.J. Cohen, D.B. Diercks, M. Moscucci, S. Ramee, T.Y. Wang, T. Connolly, J.A. Spertus, Predicting in-hospital mortality in patients with acute myocardial infarction, J. Am. Coll. Cardiol. 68 (2016) 626–635.
[9] M. Smit, A.R. Coetzee, A. Lochner, The pathophysiology of myocardial ischemia and perioperative myocardial infarction, J. Cardiothorac. Vasc. Anesth. 34 (2020) 2501–2512.
[10] Y. Kim, Y. Ahn, M.C. Cho, C.J. Kim, Y.J. Kim, M.H. Jeong, Current status of acute myocardial infarction in Korea, Kor. J. Intern. Med. 34 (2019) 1.
[11] K.C. Park, D.C. Gaze, P.O. Collinson, M.S. Marber, Cardiac troponins: from myocardial infarction to chronic disease, Cardiovasc. Res. 113 (2017) 1708–1718.
[12] J.B. Cabello, A. Burls, J.I. Emparanza, S.E. Bayliss, T. Quinn, Oxygen therapy for acute myocardial infarction, Cochrane Database Syst. Rev. 12 (2016) 1–60.

[13] S. Aydin, K. Ugur, S. Aydin, İ. Sahin, M. Yardim, Biomarkers in Acute Myocardial Infarction: Current Perspectives, Vascular Health and Risk Management, 2019, pp. 1–10.
[14] Y. Sandoval, A.S. Jaffe, Type 2 myocardial infarction: JACC review topic of the week, J. Am. Coll. Cardiol. 73 (2019) 1846–1860.
[15] M.A. Tomeh, R. Hadianamrei, X. Zhao, Silk fibroin as a functional biomaterial for drug and gene delivery, Pharmaceutics 11 (2019) 494.
[16] Z. Gharehnazifam, R. Dolatabadi, M. Baniassadi, H. Shahsavari, A.-M. Kajbafzadeh, K. Abrinia, M. Baghani, Computational analysis of vincristine loaded silk fibroin hydrogel for sustained drug delivery applications: multiphysics modeling and experiments, Int. J. Pharm. 609 (2021), 121184.
[17] O. Gianak, G.Z. Kyzas, V.F. Samanidou, E.A. Deliyanni, A review for the synthesis of silk fibroin nanoparticles with different techniques and their ability to be used for drug delivery, Curr. Anal. Chem. 15 (2019) 339–348.
[18] J. Wu, A. Zheng, Y. Liu, D. Jiao, D. Zeng, X. Wang, L. Cao, X. Jiang, Enhanced bone regeneration of the silk fibroin electrospun scaffolds through the modification of the graphene oxide functionalized by BMP-2 peptide, Int. J. Nanomed. 14 (2019) 733.
[19] J. Liu, H. Sun, Y. Peng, L. Chen, W. Xu, R. Shao, Preparation and characterization of natural silk fibroin hydrogel for protein drug delivery, Molecules 27 (2022) 3418.
[20] Z. Yin, D. Kuang, S. Wang, Z. Zheng, V.K. Yadavalli, S. Lu, Swellable silk fibroin microneedles for transdermal drug delivery, Int. J. Biol. Macromol. 106 (2018) 48–56.
[21] Y. Ma, B.S.B. Canup, X. Tong, F. Dai, B. Xiao, Multi-responsive silk fibroin-based nanoparticles for drug delivery, Front. Chem. 8 (2020), 585077.
[22] P. Kumar, G. Sharma, R. Kumar, B. Singh, R. Malik, O.P. Katare, K. Raza, Promises of a biocompatible nanocarrier in improved brain delivery of quercetin: biochemical, pharmacokinetic and biodistribution evidences, Int. J. Pharm. 515 (2016) 307–314, https://doi.org/10.1016/j.ijpharm.2016.10.024.
[23] M.M. Eshaghi, M. Pourmadadi, A. Rahdar, A.M. Diez-Pascual, Improving quercetin anticancer activity through a novel polyvinylpyrrolidone/polyvinyl alcohol/TiO2 nanocomposite, J. Drug Deliv. Sci. Technol. 81 (2023), 104304.
[24] A. Maugeri, A. Calderaro, G.T. Patanè, M. Navarra, D. Barreca, S. Cirmi, M.R. Felice, Targets involved in the anti-cancer activity of quercetin in breast, colorectal and liver neoplasms, Int. J. Mol. Sci. 24 (2023) 2952.
[25] R. Campión, C.J. Gonzalez-Navarro, A.L.M. López, M.C. Martínez-Oharriz, C. Matías, M.-J. Sáiz-Abajo, M. Collantes, I. Peñuelas, J.M. Irache, Zein-based nanospheres and nanocapsules for the encapsulation and oral delivery of quercetin, Int. J. Pharm. 643 (2023), 123216.
[26] M. Azeem, M. Hanif, K. Mahmood, N. Ameer, F.R.S. Chughtai, U. Abid, An insight into anticancer, antioxidant, antimicrobial, antidiabetic and anti-inflammatory effects of quercetin: a review, Polym. Bull. 80 (2023) 241–262.
[27] S.U. Din Wani, G.H. Veerabhadrappa, Silk fibroin based drug delivery applications: promises and challenges, Curr. Drug Targets 19 (2018) 1177–1190.
[28] S.U.D. Wani, S.P. Gautam, Z.L. Qadrie, H. V Gangadharappa, Silk fibroin as a natural polymeric based bio-material for tissue engineering and drug delivery systems-A review, Int. J. Biol. Macromol. 163 (2020) 2145–2161.
[29] S. He, L. Wu, X. Li, H. Sun, T. Xiong, J. Liu, C. Huang, H. Xu, H. Sun, W. Chen, Metal-organic frameworks for advanced drug delivery, Acta Pharm. Sin. B 11 (2021) 2362–2395.
[30] S. Rojas, F.J. Carmona, C.R. Maldonado, P. Horcajada, T. Hidalgo, C. Serre, J.A.R. Navarro, E. Barea, Nanoscaled zinc pyrazolate metal–organic frameworks as drug-delivery systems, Inorg. Chem. 55 (2016) 2650–2663.
[31] Y. Sun, L. Zheng, Y. Yang, X. Qian, T. Fu, X. Li, Z. Yang, H. Yan, C. Cui, W. Tan, Metal–organic framework nanocarriers for drug delivery in biomedical applications, Nano-Micro Lett. 12 (2020) 1–29.
[32] B. Maranescu, A. Visa, Applications of metal-organic frameworks as drug delivery systems, Int. J. Mol. Sci. 23 (2022) 4458.
[33] L. Wang, M. Zheng, Z. Xie, Nanoscale metal–organic frameworks for drug delivery: a conventional platform with new promise, J. Mater. Chem. B 6 (2018) 707–717.
[34] H.D. Lawson, S.P. Walton, C. Chan, Metal–organic frameworks for drug delivery: a design perspective, ACS Appl. Mater. Interfaces 13 (2021) 7004–7020.
[35] O. Akturk, Z. Gun Gok, O. Erdemli, M. Yigitoglu, One-pot facile synthesis of silk sericin-capped gold nanoparticles by UVC radiation: investigation of stability, biocompatibility, and antibacterial activity, J. Biomed. Mater. Res., Part A 107 (2019) 2667–2679, https://doi.org/10.1002/jbm.a.36771.
[36] D.P. Dorairaj, J. Haribabu, M. Dharmasivam, R.E. Malekshah, M.K. Mohamed Subarkhan, C. Echeverria, R. Karvembu, Ru(II)-p-Cymene complexes of furoylthiourea ligands for anticancer applications against breast cancer cells, Inorg. Chem. 62 (2023) 11761–11774, https://doi.org/10.1021/acs.inorgchem.3c00757.
[37] G. Kalaiarasi, M. Mohamed Subarkhan, C.K. Fathima Safwana, S. Sruthi, T. Sathiya Kamatchi, B. Keerthana, S.L. Ashok Kumar, New organoruthenium(II) complexes containing N, X-donor (X = O, S) heterocyclic chelators: synthesis, spectral characterization, in vitro cytotoxicity and apoptosis investigation, Inorg. Chim. Acta. 535 (2022), 120863, https://doi.org/10.1016/j.ica.2022.120863.
[38] S. Swaminathan, J. Haribabu, M.K. Mohamed Subarkhan, G. Manonmani, K. Senthilkumar, N. Balakrishnan, N. Bhuvanesh, C. Echeverria, R. Karvembu, Coordination behavior of acylthiourea ligands in their Ru(II)–Benzene Complexes─Structures and anticancer activity, Organometallics 41 (2022) 1621–1630, https://doi.org/10.1021/acs.organomet.2c00127.
[39] K. Giriraj, M.S. Mohamed Kasim, K. Balasubramaniam, S.K. Thangavel, J. Venkatesan, S. Suresh, P. Shanmugam, C. Karri, Various coordination modes of new coumarin Schiff bases toward Cobalt (III) ion: synthesis, spectral characterization, in vitro cytotoxic activity, and investigation of apoptosis, Appl. Organomet. Chem. 36 (2022), e6536, https://doi.org/10.1002/aoc.6536.
[40] M.K.M. Subarkhan, R. Ramesh, Ruthenium(ii) arene complexes containing benzhydrazone ligands: synthesis, structure and antiproliferative activity, Inorg. Chem. Front. 3 (2016) 1245–1255, https://doi.org/10.1039/C6QI00197A.
[41] M.K. Mohamed Subarkhan, L. Ren, B. Xie, C. Chen, Y. Wang, H. Wang, Novel tetranuclear ruthenium(II) arene complexes showing potent cytotoxic and antimetastatic activity as well as low toxicity in vivo, Eur. J. Med. Chem. 179 (2019), https://doi.org/10.1016/j.ejmech.2019.06.061.
[42] T. Sathiya Kamatchi, M.K. Mohamed Subarkhan, R. Ramesh, H. Wang, J.G. Małecki, Investigation into antiproliferative activity and apoptosis mechanism of new arene Ru(ii) carbazole-based hydrazone complexes, Dalton Trans. 49 (2020) 11385–11395, https://doi.org/10.1039/D0DT01476A.
[43] A. Suraiya, R. Biswas, K.P. Chennazhi, R. Jayakumar, Chitosan-hyaluronic acid/nano silver composite sponges for drug resistant bacteria infected diabetic wounds, Int. J. Biol. Macromol. 62 (2013), https://doi.org/10.1016/j.ijbiomac.2013.09.011.
[44] M. Shah, P. Kc, G. Zhang, Assessment of decellularized porcine myocardial slice as an acellular cardiac patch, ACS Appl. Mater. Interfaces 11 (2019) 23893–23900, https://doi.org/10.1021/acsami.9b06453.
[45] L. Tian, M. Wei, L. Ji, M. Zheng, G. Liu, L. Wang, Fabrication and investigation of cardiac patch embedded with gold nanowires for improved myocardial infarction therapeutics, J. Exp. Nanosci. 16 (2021) 212–228, https://doi.org/10.1080/17458080.2021.1912319.
[46] T. Su, K. Huang, M.A. Daniele, M.T. Hensley, A.T. Young, J. Tang, T.A. Allen, A.C. Vandergriff, P.D. Erb, F.S. Ligler, K. Cheng, Cardiac stem cell patch integrated with microengineered blood vessels promotes cardiomyocyte proliferation and neovascularization after acute myocardial infarction, ACS Appl. Mater. Interfaces 10 (2018) 33088–33096, https://doi.org/10.1021/acsami.8b13571.
[47] K. Chen, A. Peters, A. Schneider, =KORA Study Group, Burden of myocardial infarctions attributable to heat and cold, Eur. Heart J. 40 (2019) 3440–3441, https://doi.org/10.1093/eurheartj/ehz612.
[48] Q. Wu, M. Niu, X. Chen, L. Tan, C. Fu, X. Ren, J. Ren, L. Li, K. Xu, H. Zhong, Biocompatible and biodegradable zeolitic imidazolate framework/polydopamine nanocarriers for dual stimulus triggered tumor thermo-chemotherapy, Biomaterials 162 (2018) 132–143.
[49] D. Duan, H. Liu, M. Xu, M. Chen, Y. Han, Y. Shi, Z. Liu, Size-controlled synthesis of drug-loaded zeolitic imidazolate framework in aqueous solution and size effect on their cancer theranostics in vivo, ACS Appl. Mater. Interfaces 10 (2018) 42165–42174.